Validation and assessment of satellite-based columnar CO2 and CH4 mixing-ratios from GOSAT and OCO-2 satellites over India

Harish Gadhavi[1], Akanksha Arora[1,2], Chaithanya Jain[3], Mahesh Kumar Sha[4†], Frank Hase[5], Matthias Frey[6†], Srikanthan Ramachandran[1], Achuthan Jayaraman[3]

[1]Space and Atmospheric Science Division, Physical Research Laboratory, Ahmedabad, India
[2]Indian Institute of Technology Gandhinagar, Gandhinagar, India
[3]National Atmospheric Research Laboratory, Gadanki, India
[4]Royal Belgian Institute for Space Aeronomy, Brussels, Belgium
[5]Institute of Meteorology and Climate Research, Karlsruhe Institute of Technology, Karlsruhe, Germany
[6]National Institute for Environmental Studies, Tsukuba, Japan

[†]Formerly at Institute of Meteorology and Climate Research, Karlsruhe Institute of Technology, Karlsruhe, Germany

Correspondence to: Harish Gadhavi (hgadhavi@prl.res.in)

Abstract. The OCO-2 and GOSAT series of satellites provide near-global coverage of CO_2 and CH_4 mixing ratios. To accurately derive emission fluxes from the observed mixing ratios, it is crucial that these data meet specific precision and systematic error requirements. In this study, we report validation results for GOSAT and OCO-2 over South Asia, obtained using a portable Fourier Transform infrared Spectrometer (FTS) at a tropical rural site (Gadanki; Latitude: 13.45° N, Longitude: 79.18° E) in Southern India, from November 2015 to July 2016. Biases in CH_4 mixing ratios from GOSAT ranged from -9 to -18.5 ppb, depending on the collocation criteria, while CO_2 data from OCO-2 demonstrated better accuracy and precision, meeting the requirements of ESA's Climate Change Initiative (CCI). Using the FLEXPART model, we also show that CH_4 emissions from regional sources accounted for only 35% of the day-to-day observed variability. Both model-derived and observed mixing ratios exhibited the same seasonal variation, with higher values in October-November and lower values in June-July. However, the observed mixing ratios decreased by approximately 100 ppb, while the model-derived values decreased by only 20 ppb, suggesting that atmospheric chemistry and variations in background concentrations play a significant role over South India.

1 Introduction

Carbon dioxide (CO_2) and methane (CH_4) are the two top most important greenhouse gases (GHGs) responsible for anthropogenic global warming. While the role of CH_4 in global warming is of primary interest, CH_4 also plays an important role in atmospheric chemistry by affecting OH amount, ozone production in remote areas and water (production) in the stratosphere (Fiore et al., 2002; Fleming et al., 2015; Laughner et al., 2021; Noel et al., 2018). Both CO_2 and CH_4 abundances in the atmosphere are on continuous rise post-industrial era (Dunn et al., 2022; Turner et al., 2022) and hence a continuous global monitoring of carbon dioxide and methane is highly desirable for identifying sources, sinks, trends and effective implementation of global treaties on reduction of greenhouse gases by individual countries. Satellites due to their continuous improving data products, have come to be recognized as important tool in recent decade for monitoring and studying greenhouse gases. Satellites such as GOSAT and OCO-2 capture scattered solar radiation in the near infrared spectral region and provide columnar mixing ratios. GOSAT and OCO-2 are providing global coverage every 3 days and 15 days respectively (Table 1).

39 **Table 1. Launch date, equator crossing time, revisit time for global coverage and sensor technology of satellites, the data of**
40 **which are used in the study.**

Name of satellite/sensor	Agency responsible for launch / maintenance	Launch Date	Equator crossing time	Satellite revisit time on same location	Greenhouse Gas related Data products	Principle of measurement
GOSAT aka Ibuki	JAXA, Japan / NIES, Japan	23 January 2009	13:00	3 days	Columnar CO_2 Columnar CH_4 CO_2 profile CH_4 profile	Fourier Transform Spectrometer
OCO-2 (Orbiting Carbon Observatory - 2)	JPL, USA	July 2014	13:35	16 days	Columnar CO_2	Diffraction grating

41 Satellite based estimates of greenhouse and trace gases have proved effective for deriving the emission fluxes (Berga-
42 maschi et al., 2007, 2009; Bousquet et al., 2010; Chevallier et al., 2005). However, the improvement that can be
43 achieved in emission fluxes depends highly on the accuracy of satellite retrievals. Climate Change Initiative (CCI) pro-
44 gramme of European Space Agency (ESA) has listed the threshold precision and systematic error requirements for sat-
45 ellite derived columnar CO_2 and CH_4 mixing ratios (henceforth, columnar mixing ratios of CO_2 and CH_4 are represented
46 by symbols XCO_2 and XCH_4 respectively), which are < 8 ppm precision and < 0.5 ppm systematic error for XCO_2 indi-
47 vidual measurements, and < 34 ppb precision and < 10 ppb systematic error for XCH_4 individual measurements for
48 deriving the regional emission fluxes of these species (Chevallier et al., 2016). WMO's Global Climate Observing Sys-
49 tem (GCOS) implementation plan has listed 1-sigma accuracy requirement of < 0.5 ppm for XCO_2 and < 5 ppb for
50 XCH_4, respectively (GCOS-200, 2016).
51 To validate satellite-based estimates, standards against which the satellite observations can be compared are needed.
52 The Total Carbon Column Observing Network (TCCON) operates high-resolution ground-based Fourier transform in-
53 frared spectrometers (FTS) for providing column-averaged greenhouse gas abundances with high accuracy and preci-
54 sion. TCCON observations serve as the reference data source for satellite validation. Recently, TCCON is supplement-
55 ed by portable FTS operated in the framework of the Collaborative Carbon Column Observing Network (COCCON).
56 TCCON currently operates more than 20 stations worldwide for high precision measurements of column average dry air
57 mole fractions of CO_2, CH_4, N_2O, HF, CO, H_2O and HDO (https://tccon-wiki.caltech.edu; accessed in Sep 2024). All
58 the sites follow common set of standards for instrumentation, data acquisition, calibration and analysis as prescribed by
59 the TCCON Steering committee. TCCON sites use IFS 125HR FTS manufactured by Bruker Optics which cover a
60 spectral range from 3900 cm^{-1} to 15500 cm^{-1} with a spectral resolution of 0.02 cm^{-1}. The calibration of TCCON is
61 achieved using aircraft profiling over the sites. Typical error in XCO_2 is less than 0.2% for solar zenith angle less than
62 83° (Wunch et al., 2011a). While the XCO_2 and XCH_4 measured at TCCON sites are highly accurate and very im-
63 portant for validation of satellite, model and other instruments, the spectrometer is expensive, large and requires contin-
64 uous maintenance. The IFS 125HR FTS dimensions are of the order of 1 m x 1 m x 3 m and weighs several 100 kg,
65 restricting its wide spread use or its deployment for short field campaigns or at remote sites with limited manpower. To
66 supplement TCCON observations and to provide wider coverage of GHG observations, the Karlsruhe Institute of Tech-
67 nology (KIT) in collaboration with Bruker Optics, started developing a new type of portable FTS in 2011 which pro-

68 vides accurate measurement of GHGs while being lightweight and cost-effective. The prototype performance is de-
69 scribed in Gisi et al. (2012). The spectrometer has become commercially available since 2014 under model designation
70 EM27/SUN. Sha et al. (2020) compared the four different types of low-resolution spectrometers against IFS 125HR as
71 well as in-situ observations using AirCore from one of the TCCON site over a period of 8 months and found
72 EM27/SUN had the best performance matrix against high resolution spectrometer. COCCON is an emerging network of
73 the portable FTS which uses tested and calibrated EM27/SUN spectrometers as well as common algorithms for data
74 processing (Alberti et al., 2022; Frey et al., 2019; Sha et al., 2020). Support for calibration and data processing is pro-
75 vided by KIT and the COCCON spectrometers are calibrated against TCCON by performing side-by-side observations.
76 Today, more than 83 EM27/SUN spectrometers are operated worldwide under COCCON network (Alberti et al.,
77 2022a). The portability of EM27/SUN spectrometer and high accuracy in retrieving XCO_2 and XCH_4 have made the
78 instrument and COCCON network being used in a variety of applications. Pak et al. (2023) and Herkommer et al.
79 (2024) have used EM27/SUN spectrometer as travelling standard to evaluate consistency of TCCON measurements.
80 Frausto-Vicencio et al. (2023) have used EM27/SUN spectrometer to estimate combustion efficiency of wild fires at
81 regional scale. Stremme et al. (2023) have used the spectrometer to study CO_2 plumes from volcano. Dietrich et al.
82 (2021) and Alberti et al. (2022b) have used them for detecting city scale gradient in the gas mixing ratios and identify-
83 ing the sources of emissions.

84 An assessment conducted by Buchwitz et al. (2017) using TCCON sites found that GOSAT and OCO-2 meet the re-
85 quirements set by ESA's CCI Programme and WMO's GCOS implementation plan across various parts of the world.
86 However, due to a lack of data, this systematic assessment has so far not been conducted over South Asia. Howver,
87 there have been a few studies that compared satellite data with ground-based FTIR observations from Shadnagar
88 (17°05′ N, 78°13′ E), near Hyderabad, Telangana—a city in the south-central part of India. Sagar et al. (2022) com-
89 pared XCH_4 values from Sentinel-5P/TROPOMI (from December 2021 to March 2021) with ground-based FTIR ob-
90 servations and found a mean bias of 3.61 ppb. Pathakoti et al. (2024) compared XCO_2 data from the OCO-2 satellite
91 with ground-based FTIR and reported a mean bias of 3.81 ppm and a root mean square error (RMSE) of 6.6 ppm.
92 Pathakoti et al. (2024) used version 8 bias-corrected OCO-2 data. Aside from these few studies, no systematic ground
93 validation of satellite data for GHGs has been conducted over the South Asian region. Additionally, there has been no
94 validation of GOSAT over South Asia. Since the release of version 8 of OCO-2 data, several improvements have been
95 made to the OCO-2 algorithm, and the latest version (v11.1) is now available to public users.

96 National Atmospheric Research Laboratory (NARL), Gadanki and Institute for Meteorology and Climate Research
97 (IMK-ASF) of Karlsruhe Institute of Technology (KIT), Karlsruhe collaborated to make XCO_2 and XCH_4 measure-
98 ments over South India using a portable Fourier Transform Spectrometer (FTS) similar to the one in COCCON net-
99 work. In this manuscript, we present a systematic validation of XCO_2 and XCH_4 estimated from GOSAT and OCO-2
100 over a site in South Asia using ground-based measurements and using the latest retrieval algorithms.

2 Instrumentation and Data

102 In this study, a commercial low resolution (0.5 cm⁻¹) FTS (Model: EM27/SUN FTS Make Bruker) with modified sun-
103 tracker and InGaAs detector is used. The spectrometer has high thermal and mechanical stability and 0.5 cm⁻¹ spectral
104 resolution in the spectral range 5000 to 9000 cm⁻¹. KIT has developed a sun-tracker system that utilizes image of sun on
105 field stop of spectrometer to guide sun-tracker for accurate position of the sun. This allows far more precise sun-
106 tracking even when intensity over the sun disk is varying due to cloud or other factors. The tracking accuracy achieved
107 is of the order of 11 arc sec (Gisi et al., 2011). A detailed description of the instrument can be found in Gisi et al.

108 (2012). The instrument used has been calibrated by performing side-by-side measurements next to the TCCON spec-

109 trometer in Karlsruhe. The instrument is calibrated for specific deviations from nominal instrumental line shape (ILS)

110 and the absence of any other systematic errors is verified at KIT. Details about the ILS measurement and data analysis

111 as well as the comparison of calibration factors between the COCCON spectrometers have been discussed in Frey et al.

112 (2019), Sha et al. (2020) and Alberti et al., (2022). Sha et al. (2020) have found a mean bias of -0.18±0.45 ppm and

113 0.003±0.005 ppm between EM27/SUN and TCCON instrument for XCO_2 and XCH_4 respectively. Ratios of XCO_2 and

114 XCH_4 values estimated using the instrument unit is used in current study (Instrument Sr. No. 52) and the reference IFS

115 125HR had values of 0.999482 and 1.000825 before the start of the observations at Gadanki (Alberti et al., 2020). In

116 addition to solar spectra, measurements of atmospheric parameters like temperature and pressure were also obtained

117 near the spectrometer.

2.1 Ground-based FTS

119 The recorded spectra are analysed using retrieval code PROFFAST v2.4 developed at KIT (KIT IMK-ASF 2024a).

120 PROFFAST software retrieves the gas amount by fitting solar absorption spectra and scaling the a priori atmospheric

121 profiles of the gases. It was run using a python interface PROFFASTpylot v1.3 which also takes care of preprocessing

122 of raw instrument data (Feld et al., 2024; KIT IMK-ASF 2024b). PROFFAST algorithm is validated in several studies

123 and used across all the COCCON sites to provide uniform and consistent data processing (Frey et al., 2019; Gisi et al.,

124 2012; Hase et al., 2004; Sepúlveda et al., 2012; Sha et al., 2020). The spectral windows used for different species are

125 shown in Table **2**. The algorithm requires vertical profiles of temperature and pressure and a priori estimates of profiles

126 of species to be estimated. Vertical profiles of temperature and pressure are obtained from NCEP reanalysis data corre-

127 sponding to the dates of observations. The a priori estimates of species profiles are obtained from WACCM (Whole

128 Atmosphere Community Climate Model) (Marsh et al., 2013) which is the average of 40 year monthly mean values for

129 the site. The preprocessing step involves quality check of interferogram, DC correction, fast fourier transform, phase

130 correction and resampling of the spectra. Each record of raw data is a set of 10 spectra of which 5 are captured when the

131 mirror is moving forward and 5 are captured when the mirror is moving backward. The interferogram is checked for

132 signal level and source brightness fluctuations also known as DC variability and is removed from further analysis if

133 threshold levels are not met. The other measurement and instrument specific corrections included in the processing are

134 DC correction (correction for the sun brightness fluctuations) (Keppel-Aleks et al., 2007) and the application of instru-

135 mental line shape (ILS) parameters (Abrams et al., 1994; Alberti et al., 2020; Hase et al., 1999; Messerschmidt et al.,

136 2010). As the first step, the columnar concentrations of CO_2, CH_4, O_2 and H_2O in terms of number of molecules per m^2

137 are retrieved. Then, the CO_2 and CH_4 concentrations are converted to column average mixing ratios by assuming O_2

138 mixing ratio as 20.95% and normalising CO_2 and CH_4 concentrations with respect to O_2. This allows for compensating

139 various systematic errors. XCO_2 measurement precision is 0.13 ppmv and XCH_4 measurement precision is 0.6 ppbv

140 (Frey et al., 2019).

141 Table 2. **List of spectral windows used for retrieving columnar concentrations of various gases using ground-based FTS**

Species	Spectral windows used for analysis
CH_4	5897 – 6145 cm^{-1}
CO_2	6173 – 6390 cm^{-1}
O_2	7765 – 8005 cm^{-1}
H_2O	8353.4 – 8463.1 cm^{-1}

142 Observations were carried out from October 2015 to July 2016 in the Gadanki campus of NARL. Gadanki (Latitude:
143 13.45° N, Longitude: 79.18° E, 360 m above mean sea level) is a rural site in South India with a tropical wet climate. It
144 experiences two monsoon seasons known as southwest and northeast monsoon seasons. Change in wind circulation
145 from one season to the other season is known to have significant effect on trace-gases and aerosol concentrations at the
146 site (Renuka et al., 2014; 2020; Suman et al., 2014). The site is surrounded by hilly terrain and the nearest city is about
147 35 km away. A major part of the terrain surrounding Gadanki is forest and farm lands. Though there is no farming of
148 rice (paddy field) in the immediate vicinity, the region as a whole has a good number of paddy fields. More details
149 about the site and various atmospheric observation facility can be found in Pandit et al. (2015) and Jayaraman et al.
150 (2010). The FTS observations were carried out from morning to evening at an interval of 1 minute except during days
151 with inclement weather and weekends. More than 39,000 spectra covering a period of 10 months were analysed to re-
152 trieve XCO_2 and XCH_4.

2.2 GOSAT

154 The greenhouse gases observing satellite (GOSAT) also known as IBUKI is a joint project of the Ministry of the Envi-
155 ronment (MoE), Japan; the National Institute for Environmental Studies (NIES), Japan and the Japan Aerospace Explo-
156 ration Agency (JAXA), Japan (Yokota et al., 2009). The main instrument onboard GOSAT is a Thermal and Near infra-
157 red Sensor for carbon Observations (TANSO) (Table 1). It is a Fourier transform spectrometer (FTS) with two detec-
158 tors, one for shortwave infrared (SWIR) wavelength range and the other for thermal infrared (TIR) wavelength range
159 (Olsen et al., 2017). While the TIR sensor is used to retrieve CO_2 and CH_4 profiles, the SWIR sensor is used to retrieve
160 column average dry mole fraction of CO_2 (XCO_2) and CH_4 (XCH_4). In the current study, only XCO_2 and XCH_4 values
161 from SWIR sensor are used. The retrieval of XCO_2 is a four-step process involving pre-processing, data screening, re-
162 trieval and quality check. The pre-processing involves correction for observation time, pointing anomalies, wave-
163 number, sensor degradation, etc., and preparing meteorological data. In the second step, data are screened out for the
164 presence of cloud, high solar zenith angle (> 70°), high ground surface roughness, elevated aerosol layer, etc., along
165 with 13 instrument related quality flags. XCO_2 and XCH_4 values are then retrieved by minimizing difference between
166 observed and simulated spectra. The Goddard Earth Science Data Information and Services Center of National Aero-
167 nautics and Space Administration (NASA), USA provides XCO_2 data retrieved from GOSAT satellite's SWIR sensor
168 under Atmospheric CO_2 Observations from Space (ACOS) project (Osterman et al., 2017). In this study, FTS SWIR L2
169 v3.05 XCO_2 and XCH_4 bias corrected data products from National Institute for Environmental Studies (NIES), Japan
170 and ACOS Level 2 bias-corrected XCO_2 version v9.2 full physics retrieval data from Goddard Earth Sciences Data and
171 Information Services Center are used.

2.3 OCO-2

173 Orbiting Carbon Observatory-2 (OCO-2) is NASA's Earth remote sensing satellite to study atmospheric carbon dioxide
174 from space (Crisp et al., 2004). In the current work, we have used processed and bias corrected data version 11.1r
175 downloaded from the website of Goddard Earth Science Data Information and Services Center (GES DISC;
176 http://disc.gsfc.nasa.gov/). Version 11.1r is the latest version of data which were released in May 2023. The version
177 11.1r data contains retrospectively retrieved XCO_2 values using full physics algorithm with several improvements with
178 respect to its predecessor algorithms (Payne et al., 2023). The OCO-2 was launched on July 2, 2014 in sun-synchronous
179 orbit with equatorial crossing time at 13:30 on an ascending node with 16 days repeat cycle (Table 1). OCO-2 instru-
180 ment consists of three boresight high resolution imaging grating spectrometers which provides high resolution spectra
181 of reflected sun light in oxygen A band (0.765 µm) and in two CO_2 bands at 1.61 and 2.06 µm. The instruments can be

182 operated in three modes viz., target, glint and nadir. The ground resolution varies depending on the mode of operation.

183 In the current study, data from the nadir mode are used which has the spatial resolution of 1.29 km x 2.25 km (Crisp et

184 al., 2017). The spectra are corrected for various artefacts such as bad pixels, cosmic ray artefacts and converted to radi-

185 ometric values. Using full physics radiative transfer model, synthetic spectra are produced and compared with observed

186 spectra. An inverse model iteratively modifies the assumed atmospheric state to improve the fit. The number densities

187 of CO_2 and O_2 thus retrieved are used to get XCO_2 by taking ratio of them and multiplying it by 0.2095. The retrieval is

188 further applied bias correction obtained from collocated TCCON data (O'Dell et al., 2018). More details of the retrieval

189 process are available in Crisp et al. (2021). The OCO-2 data are distributed in two formats known as standard files and

190 Lite files. The standard files contain CO_2 mixing-ratios without bias correction whereas mixing-ratios in the Lite files

191 are bias corrected (Payne et al., 2023). The data files contain quality flag for each retrieval. The quality flag value "0"

192 corresponds to good data, whereas the quality flag value "1" suggests the presence of any of the 24 algorithmically

193 identified quality issues in the retrieved value. In the present work, we have used bias corrected data with quality flag

194 "0" only.

195 **3 FLEXPART (A Lagrangian Particle Dispersion Model)**

196 Besides, comparing satellite data with ground-based observations, we have also examined the seasonal variation of me-

197 thane mixing ratios using a Lagrangian Particle Dispersion Model to understand the influence of local sources vis-a-vis

198 long-range transport. The FLEXPART (Pisso et al., 2019), an open source model developed at NILU is widely used by

199 the research community around the world to identify the source regions of long range transport. The model takes mete-

200 orological fields as input and tracks the movement of virtual particle forward or backward in time. The particle can be

201 configured to represent a gas or aerosols of one's choice and accordingly be subjected to various physical processes

202 such as advection, turbulence, dry deposition, wet deposition, radioactive decay, etc. Except for reaction with OH radi-

203 cal no other chemical transformation is modelled in FLEXPART.

204 We configured FLEXPART for backward-in-time run from observation site (Gadanki) with virtual particle representing

205 methane molecules. The backward-in-time runs provide a source-receptor relationship which can be used to calculate

206 mixing ratios or concentrations at observation site using emission fluxes. The model run is configured such that mixing

207 ratios thus calculated represent results of emissions within the past 10 days and average of 0 to 15 km atmospheric col-

208 umn at the observation site. This configuration effectively captures most regional emissions and tropospheric methane

209 mixing ratios. Using few sensitivity tests we have found that emissions within 10 to 15 days have insignificant contribu-

210 tion to concentrations beyond 15 km. More details of the model settings used for the current study are provided in Table

211 3.

212 **Table 3. The FLEXPART model setup and the input data details**

Input Meteorological Data	ECMWF Reanalysis – Interim (ERA-Interim) (Dee et al., 2011)
Tracer	CH_4
Point of origins for retroplume (aka Release Point)	Gadanki Latitude: 13.45° N Longitude: 79.18° E, Site altitude: 365 m a. s. l. Plume release altitudes from ground: 0 – 15 km.

Number of particles released for each day	100000
Mode	Backward runs
Number of days backward for each release	10 days
User selectable Processes	Dry Deposition – disabled Convection – enabled Wet deposition – disabled Reaction with OH radical – enabled
OH reaction related settings	Constants $C = 9.65 \times 10^{-20}$ cm^3 molecule^{-1} sec^{-1} $D = 1082.0$ K $N = 2.58$ (no unit)

3.1 ECLIPSEv6 inventory

In order to calculate the concentrations resulting from recent regional emissions (emissions within past 10 days of a given observation), we used ECLIPSEv6b (**E**valuating the **CL**imate and air quality **ImP**acts of **S**hort-liv**E**d pollutants version 6b) emission inventory (Amann et al., 2011, 2012; Klimont et al., 2017; Hoglund-Isaksson, 2012; Stohl et al., 2015). The inventory is prepared following IPCC (2008) recommended method and using GAINS model (Amann et al., 2011) for 11 species including CH$_4$ across 8 economic sectors. The data are provided as 0.5° x 0.5° gridded values for the years from 1990 to 2050 at an interval of 5 years for two scenarios namely current legislation for air pollution, which is also the reference scenario and maximum technically feasible reductions scenario. The latest version (version 6b) was released in August 2019 and incorporates updates for historical data, new waste sectors, soil NO$_X$ emissions, international shipping emissions and energy-macroeconomic data. The inventory includes only anthropogenic emission fluxes from sectors viz. energy, industry, solvent use, transport, domestic combustion, agriculture, open biomass and agricultural waste burning, and waste treatment. Natural emissions from wetlands, forest fires, biogenic emissions, etc. are not included in the inventory. The total Global, South Asia (members of SAARC – South Asian Association for Regional Cooperation), and India's emissions of methane for the year 2015 were 336.2, 44.2 and 31.5 Tg, respectively.

3.2 Wetland Inventory

The emissions from wetlands can contribute significant atmospheric load of methane at the observation site and hence in addition to anthropogenic emissions from ECLIPSEv6 inventory, we used WetCHARTs version 1.0 inventory (Bloom et al., 2017a, b) for calculating methane concentrations at Gadanki from recent emissions. The inventory contains global monthly emission fluxes of methane at 0.5° by 0.5° resolution for ensemble of multiple terrestrial biosphere models, wetland extent scenarios and temperature dependencies. The emission fluxes from 2001-2015 are provided for three choices of global scaling, two choices of wetland spatial extent, two choices for temporal variability of wetland extent, nine choices of heterotrophic respiration schemes and three choices of parametrization scheme for temperature dependency. In the current work, we have used data corresponding to the scaling factor with global emissions 166 TgCH$_4$ yr^{-1}, CARDAMOM (**CAR**bon **DA**ta **MO**del fra**M**ework) terrestrial C cycle analysis for heterotrophic respiration (Bloom et al., 2016), mid-range temperature sensitivity and, spatial and temporal extent of wetlands constrained with SWAMPS (**S**urface **WA**ter **M**icrowave **P**roduct **S**eries) multi-satellite surface water product (Schroeder et al., 2015). These choices are made based on following consideration. Choice of scaling factor represents the mid-point global emissions among the three choices available viz. 124.5, 166 and 207.5 Tg CH$_4$/yr. While there are nine choices for heterotrophic respiration, there is only one choice available for emission fluxes after 2010 which is CARDAMOM and used here. Between the two choices of spatial extent and two choices of temporal variability, the SWAMP multi-

243   satellite surface water product is used because it represents observationally constrained inundated areas including lakes

244   and other water bodies.

4 Results and Discussion

246   Box plots of monthly statistics are shown in Figure 1 for (a) XCH_4 and (b) XCO_2 measured by EM27/SUN at the

247   Gadanki site. Figure 2 shows the time series of hourly mean values of XCH_4 and XCO_2 from EM27/SUN, OCO-2,

248   ACOS and GOSAT within box size ±30° longitude and ±10° latitude of the site (Table 4). A large variability in XCH_4

249   values is observed in October, but in other months, the variability is relatively low. The median values of XCH_4 are

250   found to systematically decrease from 1.892 ppm in October to 1.826 ppm in June of the following year, with similar

251   values observed in July. The monthly median values of XCO_2 increased from 396.4 ppm in October to 405.8 ppm in

252   May, then began to decrease after May. Unlike XCH_4, the XCO_2 values did not show high variability in October. A

253   similar seasonal variation was observed by Jain et al., (2021) in surface mixing ratios of CO_2 and CH_4 at Gadanki. Ka-

254   vitha and Nair (2016) using SCIAMACHY satellite data over India for the period 2003-2009, also reported similar sea-

255   sonal variations, attributing them to regional rice cultivation patterns. Further discussion on the seasonal variation is

256   provided in the subsequent section.
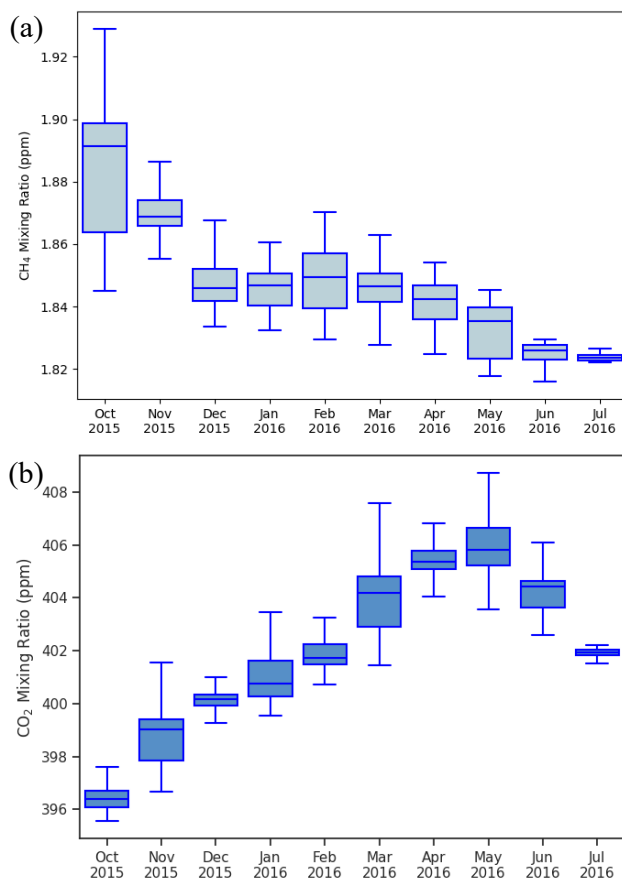
257

258   **Figure 1. Box plot of monthly statistics of (a) CH_4 and (b) CO_2 columnar mixing ratios observed at Gadanki, India using**
259   **ground-based FTIR.**

260
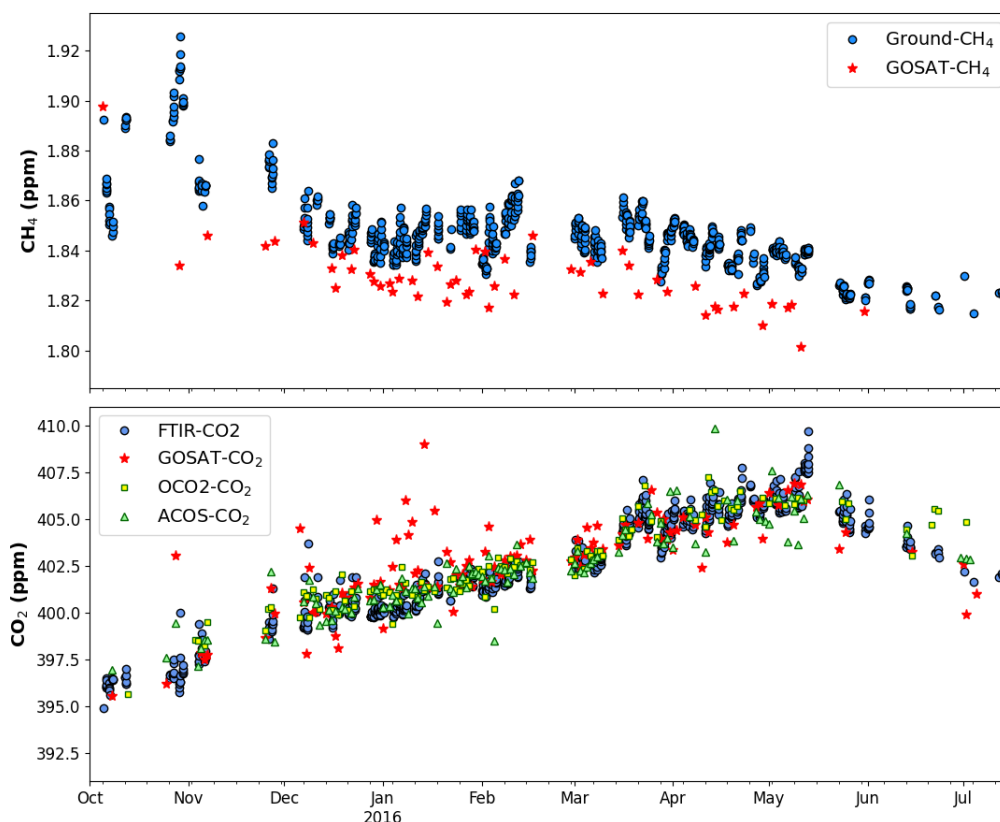
Figure 2. Hourly mean values of columnar CH$_4$ (top) and CO$_2$ (bottom) mixing ratios observed using ground based FTIR along with paired satellite observations. See the text for description of pairing method (GOSAT data version 3.05; OCO-2 data version v11.1r; ACOS v9.2; Box size ±30° longitude and ±10° latitude)

4.1 Comparison of satellite-based and ground-based mixing-ratios

The GOSAT satellite observes the same point on Earth every three days, and gas retrievals are performed only under clear sky conditions. This limits the number of concurrent observations available with ground-based FTIR. To overcome this limitation and ensure sufficient number of paired ground and satellite data for comparison, we have followed an approach similar to Buchwitz et al. (2017). This approach relies on the fact that CO$_2$ and CH$_4$ have long atmospheric residence times, allowing the history of air parcels to be used to pair data for comparison.

In this approach, the first step is to identify all satellite data within a certain distance of the ground station. Buchwitz et al. (2017) used satellite data within ±30° longitude and ±10° latitude of TCCON sites to evaluate GOSAT and OCO-2 data products. Wunch et al. (2017) used box of ±5° longitude and ±2.5° latitude around the TCCON sites in the Northern Hemisphere and ±60° longitude and ±10° latitude around the TCCON sites in the Southern Hemisphere to evaluate XCO$_2$ estimates from the OCO-2 satellite. In the second step, ground-based observations within three days of the satellite overpass and within two hours of the same time of day are paired with the satellite data. In the third step, the data pairs obtained in step 2 are further filtered using the criterion that the CAMS model output of XCH$_4$ and XCO$_2$ values, interpolated to the satellite location and ground station, cannot differ by more than 0.25 ppm for XCO$_2$ and 5 ppb for XCH$_4$, respectively. This third step is based on the premise that the CAMS model is capable of simulating transport accurately, meaning that while the absolute values may not always be correct, the spatial variability in the model is reli-

280 able. The criteria in step 3 ensures that satellite and ground values are only compared when they share the same air mass

281 history. It should be noted that the absolute value of the model simulation and its differences with observations are not

282 relevant in this step. More detailed discussions on the need and the rationale behind this complex approach for data

283 pairing can be found in Nguyen et al. (2014) and Wunch et al. (2011b).

284 We performed calculations for three different box sizes around the observation site at Gadanki (13.45° N, 79.18° E):

285 (±5° longitude, ±2.5° latitude), (±10° longitude, ±5° latitude), and (±30° longitude, ±10° latitude). By the end of the

286 third step, we obtained 55 pairs of XCH_4 from GOSAT v3.05, 117 pairs of XCO_2 from GOSAT v3.05, 118 pairs of

287 XCO_2 from ACOS v9.2 and 120 pairs of XCO_2 from OCO-2 v11.1 for the biggest box-size in Step 1 (see Table 4, Fig-

288 ure 2). The number of data pairs for XCO_2 is more than double that of XCH_4 for all box-sizes. This difference reflects

289 the fact that carbon dioxide has a much longer atmospheric lifetime (>100 years) compared to methane (~12 years).

290 **Table 4: Mean bias and scatter between satellite and ground-based measurements.**

Satellite	Species	Product version	Box Size for pairing		Number of data points	Bias = mean (Xsat - Xgrd)*	Scatter = stddev(Xsat - Xgrd)*	Pearson correlation coefficient R
			Longitude	Latitude				
GOSAT	XCH_4	v3.05	±30	±10	55	-18.5 ppb	13.8 ppb	0.47
			±10	±5	19	-9.07 ppb	12.1 ppb	0.75
			±5	±2.5	12	-12.8 ppb	6.21 ppb	0.85
	XCO_2	v3.05	±30	±10	117	0.644 ppm	1.69 ppm	0.74
			±10	±5	59	0.812 ppm	1.88 ppm	0.59
			±5	±2.5	27	0.983 ppm	1.59 ppm	0.67
		ACOS v9.2	±30	±10	118	0.163 ppm	1.09 ppm	0.90
			±10	±5	54	0.077 ppm	1.25 ppm	0.86
			±5	±2.5	38	-0.212 ppm	1.02 ppm	0.90
OCO-2	XCO_2	V11.1r	±30	±10	120	0.408 ppm	0.776 ppm	0.94
			±10	±5	67	0.342 ppm	0.806 ppm	0.94
			±5	±2.5	41	0.163 ppm	0.786 ppm	0.95

*Xsat are satellite based mixing ratio estimates and Xgrd are ground based FTIR mixing ratio estimates. For all the satellites, their bias corrected values are used.

291 With the dataset in place, we now assess the bias, scatter, and correlation between satellite and ground-based measure-

292 ments in Table 4. The bias is defined as the mean of difference between the satellite and the ground-based mixing ratio,

293 the scatter is defined as the standard deviation of the differences, and the correlation coefficient between ground and

294 satellite data is the Pearson correlation coefficient. The Climate Change Initiative (CCI) of ESA has specified precision

295 (scatter) and systematic error (bias) requirements of < 34 ppb and < 10 ppb for XCH_4 (Chevallier et al., 2016). Statisti-

296 cally significant correlation exists between ground-based and satellite measurements for all box sizes (Table 4).

297 The bias in GOSATv3.05 XCH_4 data is -9.07 ppb for the 20° x 10° longitude-latitude box size, meeting the CCI re-

298 quirement, though it was larger for the other box sizes. The scatter requirement of < 34 ppb is met with a significant

299 margin for all box sizes. The scatter ranged from 6.2 ppb to 13.8 ppb from the smallest to the largest box size.

300 The correlation between GOSAT XCO_2 and ground-based XCO_2 is significant for all the box sizes used for data pair-

301 ing. The Climate Change Initiative (CCI) of ESA has specified precision (scatter) and systematic error (bias) require-

302 ments of < 8 ppm and < 0.5 ppm for XCO_2 (Chevallier et al., 2016). The bias is lowest, at 0.644 ppm, for the largest

303 box size (60° long x 20° lat) and highest, at 0.983 ppm, for the smallest box size (10° long x 5° lat). The larger box sizes

304 correspond to the criteria set by Buchwitz et al. (2017), while the smaller box sizes correspond to Wunch et al. (2017).

305 Neither meets the CCI listed systematic error (bias) requirements of < 0.5 ppm. However, the scatter requirement of <8

306 ppm is comfortably met. The scatter values for GOSATv3.05 XCO_2 are in the range of 1.59 ppm to 1.88 ppm.

307 ACOS version 9.2 XCO_2 values, which are derived from the GOSAT satellite but use a different algorithm, perform

308 significantly better than the GOSATv3.05 values. Bias values range from -0.212 ppm to 0.163 ppm, and scatter values

309 range from 1.02 ppm to 1.25 ppm, depending on the longitude-latitude box size. The correlation for ACOS values is

310 also far superior. The correlation coefficient values for ACOS v9.2 XCO_2 are between 0.86 and 0.9, whereas the corre-

311 lation coefficient values for GOSAT v3.05 XCO_2 range from 0.59 to 0.74.

312 The correlation of ground data with OCO-2 XCO_2 is the highest among the three satellite XCO_2 datasets evaluated. The

313 correlation coefficients (R values) for OCO-2 XCO_2 v11.1r are between 0.94 and 0.95. The biases also meet the CCI

314 requirement of < 0.5 ppm, though they are slightly larger than those for ACOS XCO_2. The biases for OCO-2 XCO_2

315 range from 0.163 ppm to 0.408 ppm for different longitude-latitude boxes. The scatter for OCO-2 ranges from 0.776

316 ppm to 0.806 ppm, depending on box size, and is significantly smaller than both the GOSAT XCO_2 v3.05 and ACOS

317 XCO_2 v9.2 values, meeting the CCI criteria of <8 ppm.

318 Figure 3 shows the time series of biases for XCH_4 and XCO_2 using a ±30° × ±10° longitude-latitude box around

319 Gadanki. No systematic changes in biases are observed for both XCH_4 and XCO_2. The biases at the Gadanki location

320 are consistent with those (~ 1 ppm) reported by O' Dell et al. (2018) for OCO-2 version 8 data over TCCON sites.
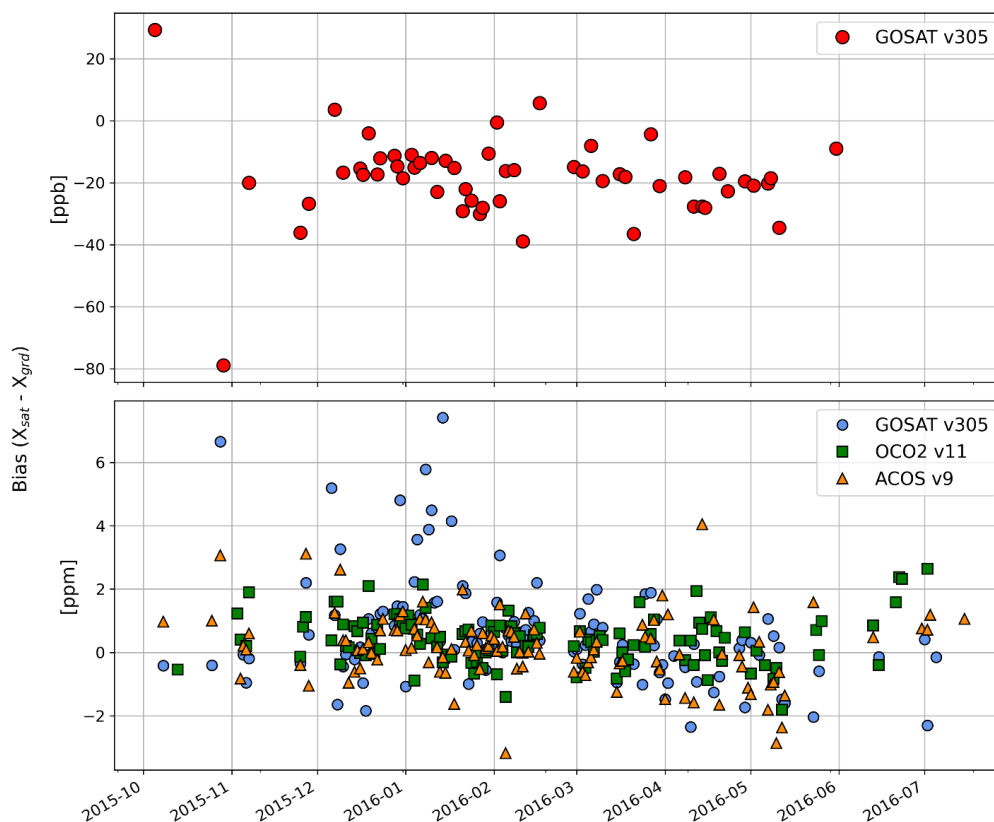
321 **Figure 3: Time series for biases in GOSAT and OCO-2 estimated XCH₄ (top) and XCO₂ (bottom) values over Gadanki, In-**
322 **dia. Values are shown for ±30° longitude and ±10° latitude box around the station.**

4.2 Case Studies and Seasonal variations

Figure 4 shows methane mixing ratio enhancements calculated using the FLEXPART model and the ECLIPSEv6+Wetland inventory. As previously mentioned, the model is configured such that the values represent day-time mean mixing-ratios in the altitude range of 0 to 15 km over Gadanki, contributed by emissions from the preceding 10 days. The altitude range of 0 to 15 km is selected because the tropopause altitude in the tropics is typically between 15 and 18 km (Pandit et al., 2014), and emissions from the past 10 days are generally confined within this range.

The 10-day back trajectory is chosen based on earlier work by Gadhavi et al. (2015), which demonstrated that, for the Gadanki location, a10-day back trajectory captures emissions from almost the entire South Asia. The averaging period is selected as daytime (9 am to 6 pm local time) to ensure a one-to-one correspondence with observed mixing ratios, which are measured using solar radiation through FTS and are therefore only available during daylight hours.

Hereafter, these values will be referred to as model values, However, it is important to note that the model values do not account for the columnar CH_4 mixing ratio resulting from emissions prior to the 10-day period and, therefore, do not represent the total columnar mixing ratio as seen in FTS or satellite data.
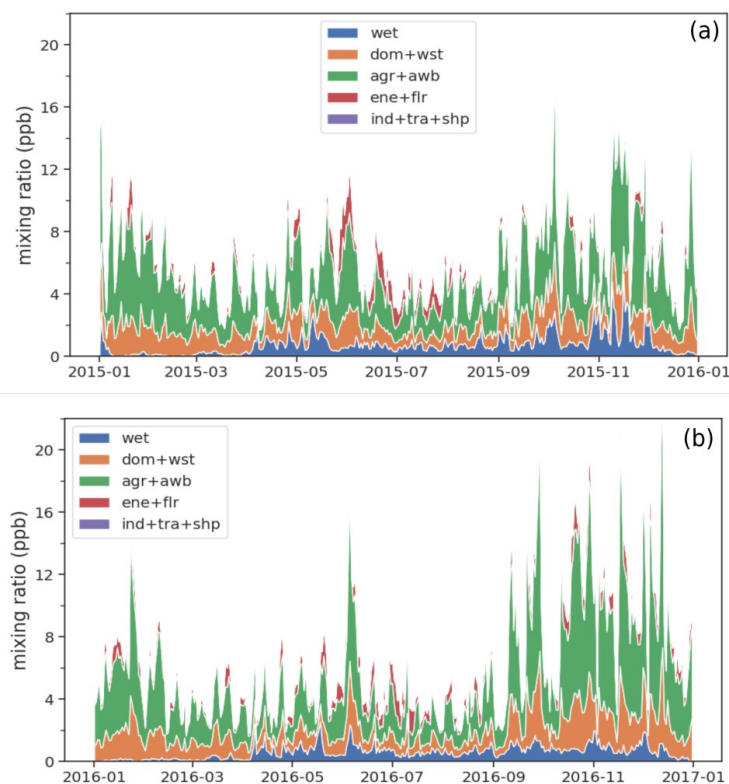
Figure 4: Model calculated columnar (0 to 15km) average methane mixing ratio enhancements due to emissions of past 10 days for year (a) 2015 and (b) 2016. Colours show contribution of different sectors viz. wetland (wet), domestic+waste (dom+wst), agriculture + agricultural waste burning (agr+awb), energy + flaring (ene+flr), and industry + transport + shipping (ind+tra+shp).

Overall, the model estimates methane mixing ratio enhancements ranging from 2 ppb to 26 ppb during 2015 and 2016.

While there is significant day-to-day variability, a seasonal pattern is still discernible in the model-calculated values.

Typically, the mixing ratio enhancements are high in November, decreases slightly in December, and rise again during

344 January and February. They decrease in March and April, briefly rise in the second half of May, and then decrease

345 again, remaining low from June to September. The mixing ratios rise again in October, peaking in November. Sector-

346 wise, wetlands do not show large seasonal variations. Wetland contributions are low from December to March. In other

347 seasons, wetland contributions occasionally reach as high as 40% of total mixing ratios, but for most part of the year,

348 they remain around 10%. The highest contribution comes from the agriculture sector, accounting for nearly 55% of the

349 total mixing ratio enhancements, followed by the waste sector, which contributes about 17% to the model values at

350 Gadanki. The domestic and energy sectors contribute about 5% each. The domestic sector's contribution is lower in

351 July and August, mainly due to the air masses originating from the west of Gadanki in peninsular India, where the

352 population is smaller and contributes less to methane emissions. Flaring contributes negligibly for most part of the year,

353 but during June to July, its contribution can reach up to 40%, primarily due to low emissions from other sectors during

354 this period and the winds from the Arabian Sea bringing emissions from oil rigs off the west coast of India, the eastern

355 Arabian Peninsula, and northeastern Africa. Industry, transport, shipping and agricultural waste burning activities con-

356 tribute less than 1% of atmospheric load of methane at Gadanki.

357 **Figure** 5 shows model-calculated methane mixing ratio (ΔXCH_4; solid blue line; left Y-axis) and the methane mixing

358 ratios (XCH_4) observed using FTS (red filled circles; right Y-axis) in a single plot. The left Y-axis represents the model

359 mixing ratio, which only accounts for emissions from the preceding 10 days. For lack of a better term, we refer to it as

360 ΔXCH_4. The right Y-axis shows the observed values in ppm. As mentioned earlier, the model was configured to reflect

361 incremental variability caused by regional emissions. If the background CH_4 mixing ratios were constant, the day-to-

362 day variability relative to background values should be the same in both the model and the observations. However, we

363 observe differences in both the absolute values of variability and their seasonal patterns. Several sudden increases in the

364 model values, which appear as spikes in **Figure** 5 (e.g. 5 October 2015 and 27 December 2015), correspond to increase

365 or decrease in the observations. While the observations are not as continuous as model values and cannot capture all the

366 variability seen in the model, some degree of day-to-day variability is correlated between the model and observations

367 ($R^2 = 0.35$). However, the magnitude of variability between the model and observed values is quite different. For in-

368 stance, the observed mixing ratios from 5 October 2015 to 8 October 2015 decreased by 49 ppb, whereas the model

369 values during the same period decreased only by 16 ppb. Over the entire observation period, observed values varied by

370 100 ppb, while the model values varied only by 20 ppb. This discrepancy may be due to two main factors: either the

371 emission fluxes in the emission inventory are underestimated, or the background mixing ratios are not constant. The

372 latter factor could explain the mismatch on a monthly scale. Starting in October 2015, both model and observed values

373 are high and decrease toward June-July 2016. While the model values are already low by March 2016, the observed

374 values decrease gradually from November 2015 to January 2016, remain nearly constant from January 2016 to April

375 2016, and then decrease rapidly in May, reaching a minimum during the last week of June and the first week of July.

376 Chandra et al. (2017) analysed methane variations over different parts of India using JAMSTEC's Atmopheric Chemi-

377 cal Transport Model. They found that, over South India, although 60% of the columnar concentration is attributed to

378 CH_4 in the lower troposphere, there is very little correlation between regional emissions and columnar methane varia-

379 tions. This was attributed to changes in atmospheric chemistry and transport. According to Chandra et al. (2017), the

380 methane loss rate increases from 6 ppb day^{-1} in January to 12 ppb day^{-1} from April to September. Additionally, anticy-

381 clonic winds in the upper troposphere confine uplifted methane molecules over broader South Asia during the monsoon

382 season, contributing significantly to methane over Western India, but not significantly over South India. Since the

383 FLEXPART doesn't include chemistry other than the reaction with OH radical, lower decrease in model values from

384 March to July could be due to absence of chemistry as well as transport of background methane above 15 km.

385
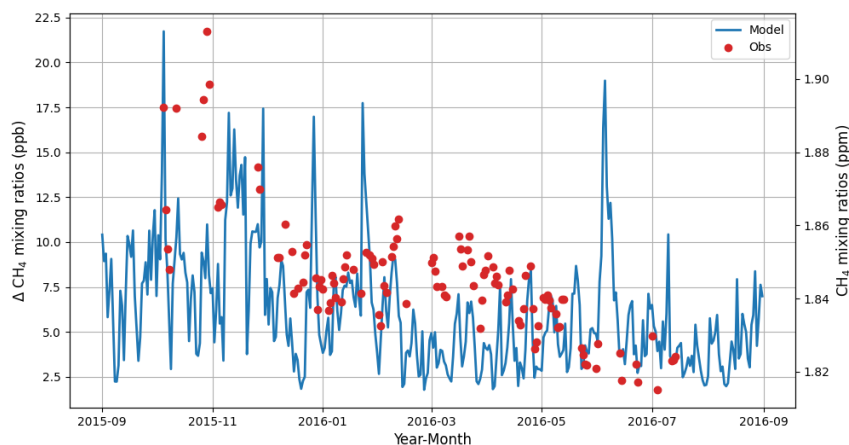
Figure 5: Observed and modelled mixing ratios at Gadanki. (The left hand y-axis shows value for modelled mixing ratio and right-hand axis shows value for observed mixing ratios

5 Conclusions and Outlook

The GOSAT and OCO-2 satellites provide global coverage of columnar mixing ratios of CO_2 and CH_4 every 3 and 15 days, respectively. These data are crucial for deriving regional greenhouse gas emission fluxes. However, the accuracy of the derived emission fluxes strongly depends on the precision and accuracy of the satellite products. In our study, we compared GOSAT and OCO-2 satellite-measured columnar mixing ratios of CO_2 and CH_4 with ground-based FTS measurements from a location in South India.

The biases in methane mixing ratios estimated using the GOSAT satellite ranged from -9 ppb to -18.5 ppb, depending on the matching criteria used for the collocation of ground and satellite footprints. These biases meet ESA's CCI requirement for systematic errors (< 10 ppb) for the smallest longitude-latitude box size. However, the bias is marginally higher than the acceptable limit for the middle box-size and does not meet the requirement for the largest box size (±30° longitude x ±10° latitude) used for matching ground and satellite pairs.

The biases in carbon dioxide mixing ratios were lowest for the ACOS v9.2 dataset among the three datasets evaluated. Both the ACOS and OCO-2 data meet ESA's CCI requirement for CO_2 biases (< 0.5 ppm), while the GOSAT v3.05 values showed higher biases, ranging from 0.644 ppm to 0.983 ppm. The precision requirement of < 8 ppm for XCO_2 set by ESA CCI was met by all three datasets with a significant margin, with scatter values ranging from 0.776 ppm to 1.88 ppm.

Our study demonstrates that satellite-based greenhouse gas estimates over South Asia show promising accuracy and precision for emission flux retrievals. In recent years, several new satellites from both public and private organizations have been launched to provide greenhouse gas estimates. This highlights the need for sustained efforts to establish a wider and denser network of Fourier Transform Spectrometer (FTS) across South Asia, which can be used for satellite and model validations with implication for better assessment of GHGs emissions and improved climate modelling.

Code availability

PROFFAST Code used to retrieve columnar concentration of GHGs from raw interferograms is publicly available. The link is provided in the main text as well as in acknowledgement section. Source code of FLEXPART model is publicly available. The link for FLEXPART is provided in the main text and in the acknowledgement section.

Data availability

Satellite data are publicly available and their links are provided in main text as well as in acknowledgement. Data of ground-based Fourier transform spectrometer will be made available through institute's website or through public repository soon. Currently, they can be obtained by writing email to HG.

Author contribution

HG, AJ, and FH conceptualised the study. HG, CJ, MS and MF did data curation. HG carried out formal analysis. HG and AA carried out model runs and analysis of model output. HG prepared visualization and wrote original draft. SR, CJ, AJ and FH reviewed and edited the draft.

Competing interests

One of the authors is a member of the editorial board of journal Atmospheric Measurement and Techniques.

Acknowledgements

Authors gratefully acknowledges following dataset and software providers and their funding agencies. Physical Research Laboratory is supported by the Department of Space, Government of India. The ERA-Interim reanalysis dataset, Copernicus Climate Change Service (C3S) available from https://www.ecmwf.int/en/forecasts/dataset/ecmwf-reanalysis-interim were used to run FLEXPART model (ECMWF, 2011), A priori profiles of pressure, temperature and species were obtained from CalTechFtp Server (https://tccon-wiki.caltech.edu/Main/ObtainingGinputData). GOSAT satellite data were obtained from NIES website http://www.gosat.nies.go.jp/. OCO-2 satellite data used in this study were produced by the OCO-2 project at the Jet Propulsion Laboratory, California Institute of Technology, and obtained from the OCO-2 data archive maintained at the NASA Goddard Earth Science Data and Information Services Center (OCO-2 Science Team, 2019). Source code of FLEXPART model was obtained from https://www.flexpart.eu. ECLIPSEv6b inventory data were provided by International Institute of Applied System Analysis through its website (https://iiasa.ac.at/models-tools-data/global-emission-fields-of-air-pollutants-and-ghgs). WetCHARTs version 1.0 – wetlands emission inventory data were provided by Oak Ridge National Laboratory's Distributed Active Archive Center (ORNL DAAC) through their web-site (https://daac.ornl.gov/). The PROFFAST v2.4 and PROFFASTpylot software are open source software developed at KIT under framework of ESA's COCCON-PROCEEDS project. These software are available at https://www.imk-asf.kit.edu/english/3225.php and https://gitlab.eudat.eu/coccon-kit/proffastpylot. Authors thank Darko Dubravica and Benedikt Herkommer for help with PROFFAST algorithm.

440 **References**

441 Abrams, M. C., Toon, G. C., & Schindler, R. A. (1994). Practical example of the correction of

442 Fourier-transform spectra for detector nonlinearity. *Appl. Opt.*, 33, 6307–6314.

443 https://doi.org/10.1364/AO.33.006307.

444 Alberti, C., Hase, F., Frey, M., Dubravica, D., Blumenstock, T., Dehn, A., et al. (2022a). Improved

445 calibration procedures for the EM27/SUN spectrometers of the COllaborative Carbon Column

446 Observing Network (COCCON). *Atmos. Meas. Tech.*, 15, 2433–2451. https://doi.org/10.5194/amt-

447 15-2433-2022.

448 Alberti, C., Tu, Q., Hase, F., Makarova, M. V., Gribanov, K., Foka, S. C., Zakharov, V.,

449 Blumenstock, T., Buchwitz, et al. (2022), Investigation of spaceborne trace gas products over St

450 Petersburg and Yekaterinburg, Russia, by using COllaborative Column Carbon Observing Network

451 (COCCON) observations, *Atmos. Meas. Tech.*, 15, 2199–2229, https://doi.org/10.5194/amt-15-

452 2199-2022.

453 Amann, M., Bertok, I., Borken-Kleefeld, J., Cofala, J., Heyes, C., Höglund-Isaksson, L., et al.

454 (2011). Cost-effective control of air quality and greenhouse gases in Europe: Modeling and policy

455 applications. *Environmental Modelling & Software*, 26, 1489–1501.

456 https://doi.org/10.1016/j.envsoft.2011.07.012

457 Amann, M., J. Borken-Kleefeld, J. Cofala, C. Heyes, Z. Klimont, P. Rafaj, P. Purohit, W. Schöpp,

458 and W. Winiwarter (2012), Future emissions of air pollutants in Europe – Current legislation

459 baseline and the scope for further reductions, TSAP Report #1, International Institute for Applied

460 Systems Analysis, Laxenburg, Austria.

461 Bergamaschi, P., C. Frankenberg, J. Meirink, M. Krol, F. Dentener, T. Wagner, U. Platt, J. Kaplan,

462 S. Körner, M. Heimann, et al. (2007), Satellite chartography of atmospheric methane from

463 SCIAMACHY on board ENVISAT: 2. Evaluation based on inverse model simulations, *J. Geophys.*

464 *Res. Atmos.*, 112, https://doi.org/10.1029/2006JD007268.

465 Bergamaschi, P., C. Frankenberg, J. F. Meirink, M. Krol, M. G. Villani, S. Houweling, F. Dentener,

466 E. J. Dlugokencky, J. B. Miller, L. V. Gatti, A. Engel, and I. Levin (2009), Inverse modeling of

467 global and regional CH4 emissions using SCIAMACHY satellite retrievals, *J. Geophys. Res.*, 114,

468 https://doi.org/10.1029/2009JD012287.

469 Bloom, A. A., Exbrayat, J.-F., van der Velde, I. R., Feng, L., & Williams, M. (2016). The decadal

470 state of the terrestrial carbon cycle: Global retrievals of terrestrial carbon allocation, pools, and

471 residence times. *Proc. Natl. Acad. Sci. U.S.A.*, 113, 1285–1290.

472 https://doi.org/10.1073/pnas.1515160113.

473 Bloom, A. A., K. W. Bowman, M. Lee, A. J. Turner, R. Schroeder, J. R. Worden, R. Weidner, K. C.

474 McDonald, and D. J. Jacob (2017a), A global wetland methane emissions and uncertainty dataset

475 for atmospheric chemical transport models (WetCHARTs version 1.0), *Geosci. Model Dev.*, 10,

476 2141–2156, https://doi.org/10.5194/gmd-10-2141-2017.

477 Bloom, A. A., K. Bowman, M. Lee, A. J. Turner, R. Schroeder, J. R. Worden, R. J. Weidner, K. C.

478 McDonald, and D. J. Jacob (2017b), CMS: Global 0.5-deg Wetland Methane Emissions and

479 Uncertainty (WetCHARTs v1.0), *ORNL DAAC*, Oak Ridge, Tennessee, USA,

480 https://doi.org/10.3334/ORNLDAAC/1502.

481 Bousquet, P., B. Ringeval, I. Pison, E. Dlugokencky, E. Brunke, C. Carouge, F. Chevallier, A.

482 Fortems-Cheiney, C. Frankenberg, D. Hauglustaine, et al. (2010), Source attribution of the changes

483 in atmospheric methane for 2006–2008, *Atmos. Chem. Phys.*, 10, 27603–27630,

484 https://doi.org/10.5194/acp-10-27603-2010.

485 Buchwitz, M., B. Dils, H. Boesch, D. Brunner, A. Butz, C. Crevoisier, R. Detmers, C. Frankenberg,

486 O. Hasekamp, W. Hewson, A. Laeng, S. Noël, J. Notholt, R. Parker, M. Reuter, O. Schneising, P.

487 Somkuti, A.-M. Sundström, and E. D. Wachter (2017), Product validation and intercomparison

488 report for essential climate variable greenhouse gases for data set climate research data package no.

489 4, *ESA Climate Change Initiative*, [Online] Available: http://www.esa-ghg-

490 cci.org/?q=webfm_send/352. (last accessed on 1 Feb 2024).

491 Chandra, N., S. Hayashida, T. Saeki, and P. K. Patra (2017), What controls the seasonal cycle of

492 columnar methane observed by GOSAT over different regions in India?, *Atmos. Chem. Phys.*, 17,

493 12633–12643, https://doi.org/10.5194/acp-17-12633-2017.

494 Chevallier, F., P. Bergamaschi, S. Houweling, T. van Leeuwen, and P. I. Palmer (2016), User

495 requirements document for the GHG-CCI project of ESA's Climate Change Initiative, *GHG-CCI*,

496 [Online] Available: http://www.esa-ghg-cci.org.

497 Chevallier, F., M. Fisher, P. Peylin, S. Serrar, P. Bousquet, F.-M. Bréon, A. Chédin, and P. Ciais

498 (2005), Inferring CO2 sources and sinks from satellite observations: Method and application to

499 TOVS data, *J. Geophys. Res. Atmos.*, 110, https://doi.org/10.1029/2005JD006390.

500 Crisp, D., R. M. Atlas, F.-M. Breon, L. R. Brown, J. P. Burrows, P. Ciais, B. J. Connor, S. C. Doney,

501 I. Y. Fung, D. J. Jacob, C. E. Miller, D. O'Brien, S. Pawson, J. T. Randerson, P. Rayner, R. J.

502 Salawitch, S. P. Sander, B. Sen, G. L. Stephens, P. P. Tans, G. C. Toon, P. O. Wennberg, S. C. Wofsy,

503 Y. L. Yung, Z. Kuang, B. Chudasama, G. Sprague, B. Weiss, R. Pollock, D. Kenyon, S. Schroll

504 (2004), The Orbiting Carbon Observatory (OCO) mission, *Adv. Space Res.*, 34, 700–709,

505 https://doi.org/10.1016/j.asr.2003.08.062.

506 Crisp, D., H. R. Pollock, R. Rosenberg, L. Chapsky, R. A. M. Lee, F. A. Oyafuso, C. Frankenberg,

507 C. W. O'Dell, C. J. Bruegge, G. B. Doran, A. Eldering, B. M. Fisher, D. Fu, M. R. Gunson, L.

508 Mandrake, G. B. Osterman, F. M. Schwandner, K. Sun, T. E. Taylor, P. O. Wennberg, and D. Wunch

509 (2017), The on-orbit performance of the Orbiting Carbon Observatory-2 (OCO-2) instrument and

510 its radiometrically calibrated products, *Atmos. Meas. Tech.*, 10, 59–81, https://doi.org/10.5194/amt-

511 10-59-2017.

512 Crisp, D., C. O'Dell, A. Eldering, B. Fisher, F. Oyafuso, V. Payne, et al. (2021), Orbiting carbon

513 observatory (OCO) - 2 Level 2 Full Physics Algorithm Theoretical Basis Document, *Jet Propulsion*

514 *Laboratory, California Institute of Technology* under contract with NASA, Pasadena, California.

515 Dee, D. P., S. M. Uppala, A. J. Simmons, P. Berrisford, P. Poli, S. Kobayashi, et al. (2011), The

516 ERA-Interim reanalysis: configuration and performance of the data assimilation system, *Q. J. R.*

517 *Meteorol. Soc.*, 137(656), 553–597, https://doi.org/10.1002/qj.828.

518 Dietrich, F., Chen, J., Voggenreiter, B., Aigner, P., Nachtigall, N., and Reger, B.: MUCCnet (2021),

519 Munich Urban Carbon Column network, *Atmos. Meas. Tech.*, 14, 1111–1126,

520 https://doi.org/10.5194/amt-14-1111-2021.

521 Dunn, R., F. Aldred, N. Gobron, et al. (2022), Global Climate, *Bull. Am. Meteorol. Soc.*, 103(8),

522 S11–S142, https://doi.org/10.1175/bams-d-22-0092.1.

523 European Centre for Medium-range Weather Forecast (ECMWF, 2011): The ERA-Interim

524 reanalysis dataset, Copernicus Climate Change Service (C3S) (accessed 30 July 2019), available

525 from https://www.ecmwf.int/en/forecasts/dataset/ecmwf-reanalysis-interim.

526 Feld, L., Herkommer, B., Vestner, J., Dubravica, D., Alberti, C., & Hase, F. (2024),

527 PROFFASTpylot: Running PROFFAST with Python. *Journal of Open Source Software*, 9, 6481,

528 https://doi.org/10.21105/joss.06481.

529 Fiore, A. M., D. J. Jacob, B. D. Field, D. G. Streets, and S. D. Fernandes (2002), Linking ozone

530 pollution and climate change: The case for controlling methane, *Geophys. Res. Lett.*, 29, 1919,

531 https://doi.org/10.1029/2002GL015601.

532 Fleming, E. L., C. George, D. E. Heard, C. H. Jackman, M. J. Kurylo, W. Mellouki, et al. (2015),

533 The impact of current CH4 and N2O atmospheric loss process uncertainties on calculated ozone

534 abundances and trends, *J. Geophys. Res. Atmos.*, 120, 5267 – 5293,

535 https://doi.org/10.1002/2014JD022067.

536 Frausto-Vicencio, I., Heerah, S., Meyer, A. G., Parker, H. A., Dubey, M., and Hopkins, F. M.

537 (2023), Ground solar absorption observations of total column CO, CO2, CH4, and aerosol optical

538   depth from California's Sequoia Lightning Complex Fire: emission factors and modified

539   combustion efficiency at regional scales, *Atmos. Chem. Phys.*, 23, 4521–4543,

540   https://doi.org/10.5194/acp-23-4521-2023.

541   Frey, M., M. K. Sha, F. Hase, M. Kiel, T. Blumenstock, R. Harig, G. Surawicz, N. M. Deutscher, K.

542   Shiomi, J. E. Franklin, H. Bösch, J. Chen, M. Grutter, H. Ohyama, Y. Sun, A. Butz, G. Mengistu

543   Tsidu, D. Ene, D. Wunch, Z. Cao, O. Garcia, M. Ramonet, F. Vogel, and J. Orphal (2019), Building

544   the COllaborative Carbon Column Observing Network (COCCON): long-term stability and

545   ensemble performance of the EM27/SUN Fourier transform spectrometer, *Atmos. Meas. Tech.*, 12,

546   1513–1530, https://doi.org/10.5194/amt-12-1513-2019.

547   Gadhavi, H. S., Renuka, K., Kiran, V. R., Jayaraman, A., Stohl, A., Klimont, Z., & Beig, G. (2015).

548   Evaluation of black carbon emission inventories using a Lagrangian dispersion model –" a case

549   study over southern India. *Atmos. Chem. Phys.*, 15, 1447–1461. https://doi.org/10.5194/acp-15-

550   1447-2015.

551   GCOS-200 (2016): The global observing system for climate: Implementation needs, *World*

552   *Meteorological Organization*.

553   Gisi, M., F. Hase, S. Dohe, and T. Blumenstock (2011), Camtracker: a new camera controlled high

554   precision solar tracker system for FTIR-spectrometers, *Atmos. Meas. Tech.*, 4, 47–54,

555   https://doi.org/10.5194/amt-4-47-2011.

556   Gisi, M., F. Hase, S. Dohe, T. Blumenstock, A. Simon, and A. Keens (2012), XCO_2 measurements

557   with a tabletop FTS using solar absorption spectroscopy, *Atmos. Meas. Tech.*, 5, 2969–2980,

558   https://doi.org/10.5194/amt-5-2969-2012.

559   Hase, F., T. Blumenstock, and C. Paton-Walsh (1999), Analysis of the instrumental line shape of

560   high-resolution Fourier transform IR spectrometers with gas cell measurements and new retrieval

561   software, *Appl. Opt.*, 38, 3417 – 3422, https://doi.org/10.1364/AO.38.003417.

562   Hase, F., J. W. Hannigan, M. T. Coffey, A. Goldman, M. Höpfner, N. B. Jones, C. P. Rinsland, and

563   S. W. Wood (2004), Intercomparison of retrieval codes used for the analysis of high-resolution,

564   ground-based FTIR measurements, *J. Quant. Spectrosc. Radiat. Transf.*, 87, 25–52,

565   https://doi.org/10.1016/j.jqsrt.2003.12.008.

566   Herkommer, B., Alberti, C., Castracane, P., Chen, J., Dehn, A., Dietrich, F., Deutscher, N. M., Frey,

567   M. M., et al. (2024), Using a portable FTIR spectrometer to evaluate the consistency of Total

568   Carbon Column Observing Network (TCCON) measurements on a global scale: the Collaborative

Carbon Column Observing Network (COCCON) travel standard, *Atmos. Meas. Tech.*, 17, 3467–3494, https://doi.org/10.5194/amt-17-3467-2024.

Hoglund-Isaksson, L. (2012), Global anthropogenic methane emissions 2005–2030: technical mitigation potentials and costs, *Atmos. Chem. Phys.*, 12, 9079–9096, https://doi.org/10.5194/acp-12-9079-2012.

IPCC 2008, 2006 IPCC Guidelines for National Greenhouse Gas Inventories – A primer, Prepared by the National Greenhouse Gas Inventories Programme, Eggleston H.S., Miwa K., Srivastava N. and Tanabe K. (eds)., IGES, Japan., 20 pp., ISBN 9784887880320.

IMK-ASF, K. (2024a, February 28). Data Processing. Retrieved from https://www.imk-asf.kit.edu/english/3225.php.

IMK-ASF, K. (2024b). PROFFASTpylot v1.3 documentation. Retrieved from https://www.imk-asf.kit.edu/english/4261.php.

Jain, C. D., V. Singh, S. T. Akhil Raj, B. L. Madhavan, and M. V. Ratnam (2021), Local emission and long-range transport impacts on the CO, CO2, and CH4 concentrations at a tropical rural site, *Atmos. Environ.*, 254, 118397, https://doi.org/10.1016/j.atmosenv.2021.118397.

Jayaraman, A., M. V. Ratnam, A. K. Patra, T. N. Rao, S. Sridharan, M. Rajeevan, et al. (2010), Study of Atmospheric Forcing and Responses (SAFAR) campaign: overview, *Annales Geophysicae*, 28, 89–101, https://doi.org/10.5194/angeo-28-89-2010.

Kavitha, M., and P. R. Nair (2016), Region-dependent seasonal pattern of methane over Indian region as observed by SCIAMACHY, *Atmos. Environ.*, 131, 316–325, https://doi.org/10.1016/j.atmosenv.2016.02.008.

Keppel-Aleks, G., G. C. Toon, P. O. Wennberg, and N. M. Deutscher (2007), Reducing the impact of source brightness fluctuations on spectra obtained by Fourier-transform spectrometry, *Appl. Opt.*, 46, 4774–4779, https://doi.org/10.1364/AO.46.004774.

Klimont, Z., K. Kupiainen, C. Heyes, P. Purohit, J. Cofala, P. Rafaj, J. Borken-Kleefeld, and W. Schöpp (2017), Global anthropogenic emissions of particulate matter including black carbon, *Atmos. Chem. Phys.*, 17, 8681–8723, https://doi.org/10.5194/acp-17-8681-2017.

Laughner, J. L., J. L. Neu, D. Schimel, P. O. Wennberg, K. Barsanti, K. W. Bowman, et al. (2021), Societal shifts due to COVID-19 reveal large-scale complexities and feedbacks between atmospheric chemistry and climate change, *Proc. Natl. Acad. Sci. U.S.A.*, 118, https://doi.org/10.1073/pnas.2109481118.

600 Messerschmidt, J., R. Macatangay, J. Notholt, C. Petri, T. Warneke, and C. Weinzierl (2010), Side

601 by side measurements of CO2 by ground-based Fourier transform spectrometry (FTS), *Tellus B:*

602 *Chem. Phys. Meteorol.*, 62, 749–758, https://doi.org/10.1111/j.1600-0889.2010.00491.x.

603 Marsh, D., M. Mills, D. E. Kinnison, and J.-F. Lamarque (2013), Climate change from 1850 to 2005

604 simulated in CESM1(WACCM), *J. Climate*, 26, 7372–7391, https://doi.org/10.1175/JCLI-D-12-

605 00558.1.

606 NCEP (2000), National Centers for Environmental Prediction/National Weather

607 Service/NOAA/U.S. Department of Commerce., NCEP FNL Operational Model Global

608 Tropospheric Analyses, continuing from July 1999. Research Data Archive at the National Center

609 for Atmospheric Research, Computational and Information Systems Laboratory. 2000 (updated

610 daily) https://doi.org/10.5065/D6M043C6. Accessed on 15 Sep 2017.

611 Noël, S., K. Weigel, K. Bramstedt, A. Rozanov, M. Weber, H. Bovensmann, and J. P. Burrows

612 (2018), Water vapour and methane coupling in the stratosphere observed using SCIAMACHY solar

613 occultation measurements, *Atmos. Chem. Phys.*, 18, 4463–4476, https://doi.org/10.5194/acp-18-

614 4463-2018.

615 OCO-2 Science Team (2019), OCO-2 Science Team/Michael Gunson, Annmarie Eldering, ACOS

616 GOSAT/TANSO-FTS Level 2 Full Physics Standard Product V9r, Greenbelt, MD, USA, Goddard

617 Earth Sciences Data and Information Services Center (GES DISC), Accessed on 1 January 2024,

618 10.5067/OSGTIL9OV0PN.

619 O'Dell, C. W., A. Eldering, P. O. Wennberg, D. Crisp, M. R. Gunson, B. Fisher, et al. (2018),

620 Improved retrievals of carbon dioxide from Orbiting Carbon Observatory-2 with the version 8

621 ACOS algorithm, *Atmos. Meas. Tech.*, 11, 6539–6576, https://doi.org/10.5194/amt-11-6539-2018.

622 Olsen, K. S., K. Strong, K. A. Walker, C. D. Boone, P. Raspollini, J. Plieninger, et al. (2017),

623 Comparison of the GOSAT TANSO-FTS TIR CH4 volume mixing ratio vertical profiles with those

624 measured by ACE-FTS, ESA MIPAS, IMK-IAA MIPAS, and 16 NDACC stations, *Atmos. Meas.*

625 *Tech.*, 10, 3697–3718, https://doi.org/10.5194/amt-10-3697-2017.

626 Osterman, G., A. Eldering, C. Cheng, C. O'Dell, D. Crisp, C. Frankenberg, and B. Fisher (2017),

627 ACOS Level 2 standard product and Lite data product data user's guide, v7.3, 51 pp.

628 Pak, N. M., Hedelius, J. K., Roche, S., Cunningham, L., Baier, B., Sweeney, C., Roehl, C.,

629 Laughner, et al. (2023), Using portable low-resolution spectrometers to evaluate Total Carbon

630 Column Observing Network (TCCON) biases in North America, *Atmos. Meas. Tech.*, 16, 1239–

631 1261, https://doi.org/10.5194/amt-16-1239-2023.

Pandit, A. K., Gadhavi, H., Ratnam, M. V., Jayaraman, A., Raghunath, K., and Rao, S. V. B. (2014).
Characteristics of cirrus clouds and tropical tropopause layer: Seasonal variation and long-term
trends. *J Atmos and Solar-Terrestrial Phys*, 121, 248–256,
https://doi.org/10.1016/j.jastp.2014.07.008

Pandit, A. K., H. S. Gadhavi, M. V. Ratnam, K. Raghunath, S. V. B. Rao, and A. Jayaraman (2015),
Long-term trend analysis and climatology of tropical cirrus clouds using 16 years of lidar data set
over Southern India, *Atmos. Chem. Phys.*, 15, 13833–13848, https://doi.org/10.5194/acp-15-13833-
2015.

Pathakoti, M., D.V., M., A.L., K., K.S., R., Taori, A., Bothale, R. V., & Chauhan, P. (2024),
Temporal variability of atmospheric columnar CO_2, CH_4, CO and N_2O concentrations using ground-
based remote sensing FTIR Spectrometer, *Advances in Space Research*, 73, 4967–4975,
https://doi.org/10.1016/j.asr.2024.02.028.

Payne, V., A. Chatterjee, R. Rosenberg, M. Kiel, B. Fisher, L. Dang, et al. (2023), Orbiting carbon
observatory-2 & 3 (OCO-2 & OCO-3) Data Product User's Guide, Operational Level 2 Lite Files,
Jet Propulsion Laboratory, California Institute of Technology, Pasadena, California.

Pisso, I., E. Sollum, H. Grythe, et al. (2019), The Lagrangian particle dispersion model FLEXPART
version 10.4, *Geosci. Model Dev.*, 12, 4955–4997, https://doi.org/10.5194/gmd-12-4955-2019.

Renuka, K., H. Gadhavi, A. Jayarman, S. V. B. Lal, M. Naja, and S. V. B. Rao (2014), Study of
ozone and NO2 over Gadanki - a rural site in South India, *J. Atmos. Chem.*, 71, 95–112,
https://doi.org/10.1007/s10874-014-9284-y.

Renuka, K., H. Gadhavi, A. Jayaraman, S. V. B. Rao, and S. Lal (2020), Study of mixing ratios of
SO2 in a tropical rural environment in south India, *J. Earth Syst. Sci.*, 129,
https://doi.org/10.1007/s12040-020-1366-4.

Rodgers, C. D. (2000), Inverse Methods for Atmospheric Sounding: Theory and Practice, *Series on
Atmospheric, Oceanic and Planetary Physics*, World Scientific Publishing Company.

Sagar, V. K., Pathakoti, M., D.V., M., K.S., R., M.V.R., S. S., Hase, F., et al. (2022), Ground-based
remote sensing of total columnar CO_2, CH_4 and CO using EM27/SUN FTIR spectrometer at a
suburban location (Shadnagar) in India and validation of Sentinel-5P/TROPOMI, *IEEE Geoscience
and Remote Sensing Letters*, 19, 1–5, https://doi.org/10.1109/LGRS.2022.3171216.

Schroeder, R., K. C. McDonald, B. D. Chapman, K. Jensen, E. Podest, Z. D. Tessler, et al. (2015),
Development and evaluation of a multi-year fractional surface water data set derived from

active/passive microwave remote sensing data, *Remote Sensing*, 7, 16688–16732, https://doi.org/10.3390/rs71215843.

Sepúlveda, E., M. Schneider, F. Hase, O. E. Garcia, A. Gomez-Pelaez, S. Dohe, T. Blumenstock, and J. C. Guerra (2012), Long-term validation of tropospheric column-averaged CH_4 mole fractions obtained by mid-infrared ground-based FTIR spectrometry, Atmos. Meas. Tech., 5, 1425–1441, https://doi.org/10.5194/amt-5-1425-2012.

Sha, M., M. de Maziere, J. Notholt, T. Blumenstock, et al. (2020), Intercomparison of low- and high-resolution infrared spectrometers for ground-based solar remote sensing measurements of total column concentrations of CO_2, CH_4 and CO, *Atmos. Meas. Tech.*, 13, 4791–4839, https://doi.org/10.5194/amt-13-4791-2020.

Stohl, A., B. Aamaas, M. Amann, et al. (2015), Evaluating the climate and air quality impacts of short-lived pollutants, *Atmos. Chem. Phys.*, 15, 10529–10566, https://doi.org/10.5194/acp-15-10529-2015.

Suman, M. N. S., H. Gadhavi, V. Ravi Kiran, A. Jayaraman, and S. V. B. Rao (2014), Role of coarse and fine mode aerosols in MODIS AOD retrieval: a case study over southern India, *Atmos. Meas. Tech.*, 7, 907–917, https://doi.org/10.5194/amt-7-907-2014.

Turner, A. J., C. Frankenberg, and E. A. Kort (2019), Interpreting contemporary trends in atmospheric methane, *Proc. Natl. Acad. Sci. U.S.A.*, 116, 2805–2813, https://doi.org/10.1073/pnas.1814297116.

Wunch, D., G. C. Toon, J.-F. Blavier, R. A. Washenfelder, J. Notholt, B. J. Connor, et al. (2011a), The Total Carbon Column Observing Network, *Philos. Trans. R. Soc. A Math. Phys. Eng. Sci.*, 369, 2087–2112, https://doi.org/10.1098/rsta.2010.0240.

Wunch, D., P. O. Wennberg, G. Osterman, B. Fisher, B. Naylor, C. M. Roehl, et al. (2017), Comparisons of the Orbiting Carbon Observatory-2 (OCO-2) XCO2 measurements with TCCON, *Atmos. Meas. Tech.*, 10, 2209–2238, https://doi.org/10.5194/amt-10-2209-2017.

Yokota, T., Yoshida, Y., Eguchi, N., Ota, Y., Tanaka, T., Watanabe, H., and Maksyutov, S. (2009), Global concentrations of CO_2 and CH_4 retrieved from GOSAT: First preliminary results. *Sola*, 5, 160–163, https://doi.org/10.2151/sola.2009-041.